23rd ABCM International Congress of Mechanical Engineering
December 6-11, 2015, Rio de Janeiro, RJ, Brazil

TRANSIENT HEAT TRANSFER ANALYSIS IN SUPERCRITICAL FLUIDS

Amanda Furtado Pinheiro
Leonardo S. de B. Alves
Laboratório de Mecânica Teórica e Aplicada, Departamento de Engenharia Mecânica, Universidade Federal Fluminense, Rua Passo da Pátria 156, Bloco E, Sala 216, Niterói, RJ 24210-240, Brazil.
amandafp@id.uff.br
leonardo.alves@mec.uff.br

Abstract. *The supercritical fluids have shown remarkable effects in physics and hydrodynamics, which take advantage of the unique properties of supercritical fluids. The heat transfer into a one dimensional cavity containing a supercritical fluid at zero gravity occurs unexpectedly fast. This phenomenon, called as piston effect, will be analyzed for different cases. A thermodynamic model for this specific happening will be used, and it consists in the general heat equation with an addition source term containing the bulk temperature time derivative. The normal expression for the piston effect relaxation time t_{PE} for this model is $t_{PE} = t_D/(\gamma - 1)^2$, where t_D is the thermal diffusion relaxation time and γ is the ratio between specific heats. Motivated by the fact that this formulation is an approximate solution, a previous work showed, for different boundary conditions for the piston effect, that the correct piston effect relaxation time should be $t_{PE} = t_D/\gamma$ instead, cause is rigorously satisfied by the exact solution when Dirichlet boundary conditions are imposed. A previous work of the same group employed Dirichlet, Neumann and Robin boundary conditions on the left wall, with prescribed temperature on the right wall in all three cases. As a continuation of this study, is intended to analyze again the heat transfer using the exact solution for three different boundary conditions for the right wall: Dirichlet, Neumann and Robin, with temperature prescribed on the left wall for all of the cases.*

Keywords: *Supercritical Fluids, Piston Effect, Relaxation Time, Heat Transfer, Thermodynamics*

1. INTRODUCTION

The heat transfer into a one dimensional cavity containing a supercritical fluid at zero gravity occurs unexpectedly fast, and it's called as piston effect. The thermal diffusivity goes to zero at the critical point and, therefore, for a long time it was believed that near the critical point there would be a sudden decrease in thermal relaxation, resulting in a very small heat transfer where the dominant type of heat exchange was heat conduction (Teixeira and de B. Alves, 2015). Then this phenomenon was explained by the existence of another type of heat transfer: being produced by convection effect. For supercritical fluids, a small change in temperature leads to a wide variation in specific gravity causing convection currents. These flows were long considered the reason for rapid heat transfer in supercritical fluids, until low gravity experiments showed similar results (Nitsche and Straub, 1987).

The piston effect remained unexplained until 1990, when a theoretical analysis (Boukari *et al.*, 1990; Onuki *et al.*, 1990) showed that a small disruption in the temperature of one of the walls of the cavity generates a thermal boundary layer at the wall of the cavity. The heated fluid from the boundary layer region undergoes an expansion, and in the case of supercritical fluid, this expansion is stronger. That expansion causes a compression in the rest of the fluid, resulting in a difference in pressure and density inside the cavity. A thermoacoustic wave shape due to these differences, and propagates into the cavity at the speed of sound. When the wave passes the boundary layer, it carries with it the present thermal energy, and distributes it to the rest of the fluid in its spread. This effect is responsible for the smooth and rapid increase in global temperature of the fluid (Zappoli, 2003; Barmatz *et al.*, 2007; Carlès, 2010).

The original thermodynamic model developed for the supercritical heat transfer in microgravity conditions is primarily the heat conduction equation with a term proportional to the temporal derivative of the global temperature (Boukari *et al.*, 1990; Onuki *et al.*, 1990). This source term models the adiabatic compression mechanism responsible for the piston effect. It becomes dominant when $\gamma >>> 1$, (near the critical point) and disappears when $\gamma = 1$ (incompressible limit).

One solution to this equation, including variables properties obtained from the literature, was first generated by numerical methods. However, global temperatures are obtained by numerical integration of the temperature field over the entire volume for each time step. Such an approach can become burdensome to two and three-dimensional areas. To work around this problem, it was proposed an alternative approximation, which replaces the volume integral for a surface integral using the Boundary Element Method.

A further solution to this equation, considering now constant properties was obtained first with an approximate Fourier transformation procedure. To reproduce this recent microgravity experiment (Nitsche and Straub, 1987), Onuki and Ferrell (1990), it is considered a fluid initially at T_0, bounded by solid walls, which have their temperature suddenly increased to

T_1. The Fourier transformation is used to get

$$T_b(t) = T_0 + \Delta T \left(1 - \exp\left[\frac{t}{t_{PE}}\right] \mathrm{erfc}\left[\sqrt{\frac{t}{t_{PE}}}\right]\right) , \tag{1}$$

for the bulk temperature, where $\Delta T = T_1 - T_0$, t_{PE} is the piston effect relation time defined as

$$t_{PE} = \frac{t_D}{(\gamma - 1)^2} , \tag{2}$$

Where $\gamma = C_P/C_V$ and C_V is the specific heat at constant volume. Although both studies consider the constant heating border, the approximate Fourier procedure has been extended to pulsed heating (Ferrell and Hao, 1993) and unsteady also (Garrabos *et al.*, 1998) . Another authors reproduced this to include two dimensions as well as curvature effects (Carlès *et al.*, 2005). They employed Separation of Variables and Laplace transform with numerical inversion to solve the governing equations, but they propose expression $t_{PE} = t_D/\gamma^2$ instead of expression (1), with t_D based on the cylinder diameter as characteristic length. This new expression implies $t_{PE} < t_D$ for $\gamma > 1$, in contradiction with $\gamma > 2$ for expression (1). Indeed, the latter implies that $t_{PE} > t_D$ for $1 < \gamma < 2$, which has not been observed in thermo-acoustic simulations and experiments under atmospheric conditions (Huang and Bau, 1997).

The focus of this paper is to use the same thermodynamic model using an exact solution, which is obtained with a generalized version (Cotta, 1993) of the classical integral transform technique (Özisik, 1993), with a standard filtering technique (Mikhailov and Özisik, 1984) and the matrix exponential function (Moler and Loan, 2003), where the eigenvalues are computed symbolically using *Mathematica*.

2. MATHEMATICAL MODEL

The classic and dimensionless thermodynamic model which solves the problem of a supercritical fluid contained within a cavity in a one-dimensional ambience without gravity is:

$$\frac{\partial \top}{\partial \tau} - \left(1 - \frac{1}{\gamma}\right) \frac{d}{d\tau} \left(\int_0^1 \top \, d\xi \right) = \frac{\partial^2 \top}{\partial \xi^2} \quad , \tag{3}$$

The initial and boundary conditions for temperature are:

$$\top(\xi, 0) = 0 \quad , \quad - \left.\frac{\partial \top}{\partial \xi}\right|_{\xi=0} + \mathcal{L}_1 \top(0,\tau) = \mathcal{L}_2 \quad \text{and} \quad \left.\frac{\partial \top}{\partial \xi}\right|_{\xi=1} + \mathcal{R}_1 \top(1,\tau) = \mathcal{R}_2 \quad , \tag{4}$$

where $\mathcal{L}_1$, $\mathcal{L}_2$, $\mathcal{R}_1$ and $\mathcal{R}_2$ are parameters that define all nine possible combinations between Dirichlet, Neumann and Robin boundary conditions. The equations are based on dimensionless variables

$$\tau = \frac{t}{t_D} \quad , \quad \xi = \frac{x}{l} \quad \text{and} \quad \top = \left(\frac{\mathcal{L}_1^* + \mathcal{R}_1^* + \mathcal{L}_1^* \mathcal{R}_1^*}{\mathcal{L}_2^* \mathcal{R}_1^* - \mathcal{L}_1^* \mathcal{R}_2^*}\right) T - \left(\frac{\mathcal{L}_2^* + \mathcal{R}_2^* + \mathcal{L}_1^* \mathcal{R}_2^*}{\mathcal{L}_2^* \mathcal{R}_1^* - \mathcal{L}_1^* \mathcal{R}_2^*}\right) \quad , \tag{5}$$

where $\mathcal{L}_1^*$, $\mathcal{R}_1^*$, $\mathcal{L}_2^*$ and $\mathcal{R}_2^*$ are related to the dimensional versions of their respective parameters without asterisks.

Table 1. Possible left wall boundaries

Boundary Type	Dirichlet	Neumann	Robin
Boundary Condition	$\top(0,\tau) = 1$	$- \left.\frac{\partial \top}{\partial \xi}\right\|_{\xi=0} = 1$	$- \left.\frac{\partial \top}{\partial \xi}\right\|_{\xi=0} + Bi \top(0,\tau) = 1 + Bi$
Boundary Constants	$\mathcal{L}_1 = \mathcal{L}_2 = \infty$	$\mathcal{L}_1 = 0$ & $\mathcal{L}_2 = 1$	$\mathcal{L}_1 = Bi$ & $\mathcal{L}_2 = 1 + Bi$

It will be analyzed the heat transfer for three different boundary conditions for the right wall: Dirichlet, Neumann and Robin, with temperature prescribed at at T_1 on the left wall for all of the cases. This choice leads to $\mathcal{L}_1 = \mathcal{L}_2 = \infty$, that means Dirichlet at the left wall, as it can be seen at Table 1. There is a restriction on the choice of $\mathcal{R}_1$ and $\mathcal{R}_2$, so that all boundary conditions will satisfy the same steady-state solution, given by:

$$\top(\xi, \infty) = 1 - \xi \quad , \tag{6}$$

which leads to the three boundary condition scenarios. Such restriction can be seen in Table 2. These conditions are controlled by a single parameter named Bi and often referred to as Biot number.

Table 2. Three right wall boundaries analyzed in the present study using $\top(0,\tau) = 1$ at the left wall.

Boundary Type	Dirichlet	Neumann	Robin
Boundary Condition	$\top(1,\tau) = 0$	$\frac{\partial \top}{\partial \xi}\Big\|_{\xi=1} = -1$	$\frac{\partial \top}{\partial \xi}\Big\|_{\xi=1} + Bi\,\top(1,\tau) = -1$
Boundary Constants	$\mathcal{R}_1 = \infty$ & $\mathcal{R}_2 = 0$	$\mathcal{R}_1 = 0$ & $\mathcal{R}_2 = -1$	$\mathcal{R}_1 = Bi$ & $\mathcal{R}_2 = -1$

In a first moment, the condition for the right wall will be Robin. This leads to $\mathcal{R}_1 = Bi$ and $\mathcal{R}_2 = -1$. It is important to note that, for Robin condition, if $Bi \to \infty$, the condition turns to Dirichlet, and if $Bi = 0$, the condition turns to Neumann.

3. SOLUTION PROCEDURE

3.1 Filtering

First, a filter is applied. Not only to separate the stationary state from the transient (Mikhailov and Özisik, 1984), but also to improve the convergence rates and to remove non-homogeneous boundary conditions. Hence, definition

$$\top(\xi,\tau) = \Theta(\xi) + \theta(\xi,\tau) \quad , \tag{7}$$

is employed here. The filter term is defined as the temperature distribution state equation, as follows:

$$\Theta(\xi) \; = \; \top(\xi,\infty) \quad , \tag{8}$$

Substituting relation (8) into governing equation (3) leads to

$$\frac{\partial \theta}{\partial \tau} - \left(1 - \frac{1}{\gamma}\right) \frac{d}{d\tau} \int_0^1 \theta \, d\xi \; = \; \frac{\partial^2 \theta}{\partial \xi^2} \quad , \tag{9}$$

which conducts the global transient behavior $\theta(\xi,\tau)$ of the model problem (3). Doing the same for the boundary conditions (4), it takes the following result:

$$\theta(\xi,0) \; = \; \xi \, - \, 1 \quad , \quad \frac{\partial \theta}{\partial \xi}\bigg|_{\xi=1} + \, Bi\,\theta(1,\tau) = 0 \quad \text{and} \quad \theta(1,\tau) = 0 \quad , \tag{10}$$

3.2 Integral Transformation

In order to separate the spatial dependencies and temporal model is proposed a solution to (9) and (10). The same is shown below:

$$\theta(\xi,\tau) \; = \; \sum_{i=1}^{\infty} \tilde{\psi}_i(\xi)\, \bar{\theta}_i(\tau) \quad , \tag{11}$$

The GITT system uses eigenvalues and eigenfunctions to solve the problem where it is applied. In this proposed solution such elements already appear. The eigenfunction provided by the auto system and the boundary conditions of the system can be viewed as follows:

$$\frac{d^2 \psi_i}{d\xi^2} \, + \, \beta_i^2 \, \psi_i(\xi) \; = \; 0 \quad , \quad \frac{d\psi_i}{d\xi}\bigg|_{\xi=1} + \, Bi\,\psi_i(1) \; = \; 0 \quad \text{and} \quad \psi_i(0) \; = \; 0 \quad , \tag{12}$$

Thus, the eigenfunctions are generated and represented by:

$$\psi_i(\xi) \; = \; \sin[\,\beta_i \, \xi\,] \quad , \tag{13}$$

and the transcendental equation is:

$$\beta_i \, \cos[\,\beta_i\,] + \, Bi \, \sin[\,\beta_i\,] \, = \, 0 \quad , \tag{14}$$

where $i = 1\,,\,2\,,\,\ldots\,,\,\infty$ provides the eigenvalues. As eigenfunctions are orthogonal, the integral transformed temperature coefficients can be set. Such a definition is shown below:

$$\bar{\theta}_i(\tau) \;=\; \int_0^1 \tilde{\psi}_i(\xi)\,\theta(\xi,\tau)\,d\xi \quad , \tag{15}$$

In this case, the norm is given by (16) (Özisik, 1993), and it is used to normalize functions $\tilde{\psi}_i = \psi_i/\sqrt{N_i}$:

$$N_i \;=\; \int_0^1 \psi_i(\xi)^2\,d\xi \;=\; \frac{Bi\,+\,Bi^2\,+\,\beta_i^2}{2\,(Bi^2+\beta_i^2)} \quad , \tag{16}$$

In order to generate a system of equations that governs the behavior of the temperature coefficients, the (9) is used. If we multiply this equation by $\tilde{\psi}_i$, integrate the result over the dimensionless cavity length and apply the transformation (15), we get:

$$\frac{d\bar{\theta}_i}{d\tau} - \eta_i\left(1-\frac{1}{\gamma}\right)\frac{d\theta_b}{d\tau} \;=\; \int_0^1 \tilde{\psi}_i(\xi)\,\frac{\partial^2\theta}{\partial\xi^2}\,d\xi\,, \tag{17}$$

where integral transform coefficient and bulk temperature are, repectively:

$$\eta_i \;=\; \int_0^1 \tilde{\psi}_i(\xi)\,d\xi \;=\; \frac{1-\cos[\,\beta_i\,]}{\beta_i\,\sqrt{N_i}} \quad \text{and} \quad \theta_b(\tau) \;=\; \int_0^1 \theta(\xi,\tau)\,d\xi \quad . \tag{18}$$

Now, if we integrate the right side of (17) by parts, apply boundary conditions in (10), substitute the equation in (12) and then use the integral transform definition (15) into the result, we get:

$$\int_0^1 \tilde{\psi}_i(\xi)\,\frac{\partial^2\theta}{\partial\xi^2}\,d\xi \;=\; \int_0^1 \frac{d^2\tilde{\psi}_i}{d\xi^2}\,\theta(\xi,\tau)\,d\xi \;=-\,\beta_i^2\int_0^1 \tilde{\psi}_i(\xi)\,\theta(\xi,\tau)\,d\xi \;=\; -\,\beta_i^2\,\bar{\theta}_i(\tau) \quad , \tag{19}$$

This related above equation can be replaced in the right side of equation (17), using the inverse definition (15) in the non-transformed bulk temperature term. Thus, there are obtained:

$$\sum_{j=1}^{\infty} A_{i,j}\,\frac{d\bar{\theta}_j}{d\tau} \;+\; \beta_i^2\,\bar{\theta}_i(\tau) \;=\; 0 \quad \text{where} \quad A_{i,j} \;=\; \delta_{i,j} \;-\; \left(1-\frac{1}{\gamma}\right)\eta_i\,\eta_j \quad , \tag{20}$$

where $i\;=\;1\,,\,2\,,\,\ldots\,,\,\infty$ and $\delta_{i,j}$ represents the Kronecker delta. It is important to notice that this integral transform equation is subject to initial transformed condition, obtained by performing a process of transformation similar to the initial condition in equation (10):

$$\bar{\theta}_i(0) \;=\; \int_0^1 (\xi-1)\,\tilde{\psi}_i(\xi)\,d\xi \;=\; -\,(1+Bi)\,\frac{\sin[\,\beta_i\,]}{\beta_i^2\,\sqrt{N_i}} \;=\; \frac{1+Bi}{Bi}\;\frac{\cos[\,\beta_i\,]}{\beta_i\,\sqrt{N_i}} \quad , \tag{21}$$

In equation (21) we have two options for Biot number: $Bi\to 0$ and $Bi\to\infty$. If we solve system (20) with initial conditions (21) for the integral transformed temperature coefficients, we can get the exact solution by combining them with relations (6) to (8) and (11):

$$\top(\xi,\tau) \;=\; 1 \;-\; \xi \;+\sum_{i=1}^{\infty} \tilde{\psi}_i(\xi)\,\bar{\theta}_i(\tau) \quad , \tag{22}$$

where its bulk value, according to the definition in (18), becomes

$$\top_b(\tau) \;=\; \int_0^1 \top(\xi,\tau)\,d\xi \;=\; \frac{1}{2} \;+\sum_{i=1}^{\infty} \eta_i\,\bar{\theta}_i(\tau) \quad . \tag{23}$$

4. RESULTS AND DISCUSSION

At this stage the results will be analyzed using the model presented above. All graphs were plotted using Wolfram MATHEMATICA version 9.0. As stated earlier, the case study is the temperature held fixed on the left wall. On the right wall, three boundary conditions are used, only three scenarios are possible. These possibilities are shown in the table 2.

Graphs were then made with the first boundary condition, so, Dirichlet on both walls for different time intervals. Several $\top$ by ξ graphics were plotted, only varying γ. The last factor can be considered as a way to determine the compressibility of the fluid due to the proximity of the critical point, or in other words, the greater the γ, the more compressible the fluid and closer to the critical point it is.

As expected, it was observed that the piston effect is best seen in more compressible fluids, as the thermal boundary layer expands more strongly. The increased γ also generates an increase in fluid bulk temperature time. So that it stay clear the action of the piston effect, several curves were made on the same graphic, varying only the characteristic time of the piston effect between $t/t_{PE} = 10^{-3}, 10^{-2}, 10^{-1}$ and 1. Below the graphs for these boundary conditions, varying γ for $2, 5, 10$ and 20.

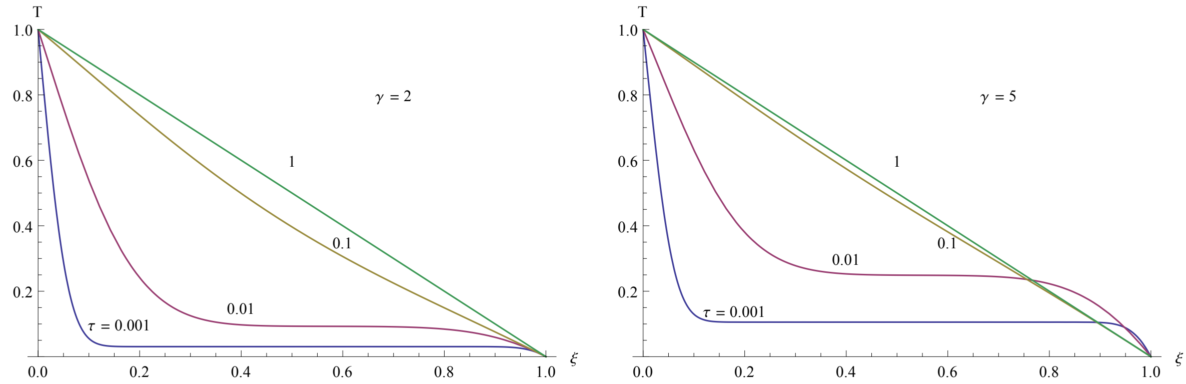

Figure 1. Local temperature profiles for a Dirichlet boundary condition at the right wall. $\gamma = 2$ (left) and $\gamma = 5$ (right)

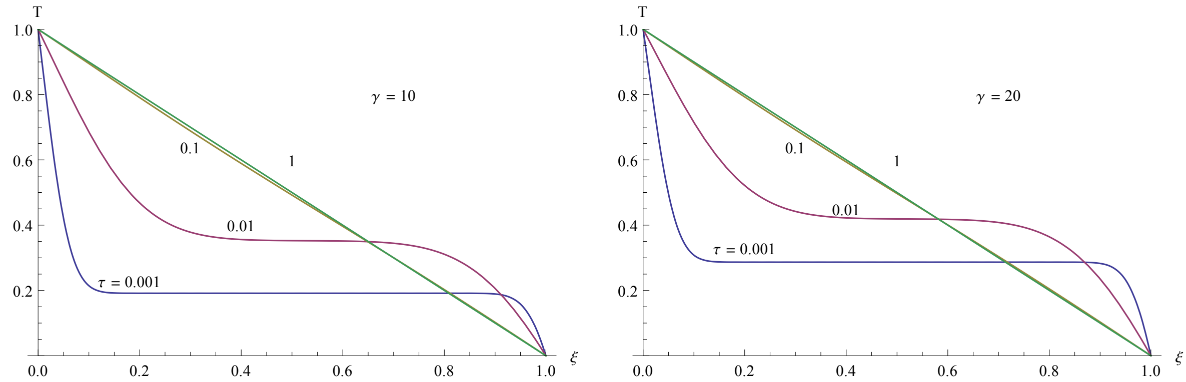

Figure 2. Local temperature profiles for a Dirichlet boundary condition at the right wall. $\gamma = 10$ (left) and $\gamma = 20$ (right)

In the above figures, we can see that in the range between $\xi = 0$ and $\xi = 0.3$, and between $\xi = 0.8$ and $\xi = 1$ there is a large temperature gradient. This gradient shows the presence of the thermal boundary layer in these regions, while in the rest of the fluid the temperature grew evenly. This uniformity is due to the presence of the piston effect, in other words, when a small temperature difference between the walls is induced, a large pressure variation is caused by the expansion of the thermal boundary layer to the remainder of the fluid, generating acoustic waves that propagate through the cavity, and successively reflected on the walls of the cavity losing energy as heat and thus warming up the fluid uniformly. This spread is not simulated, but shaped by the term containing the derivative in the bulk temperature time.

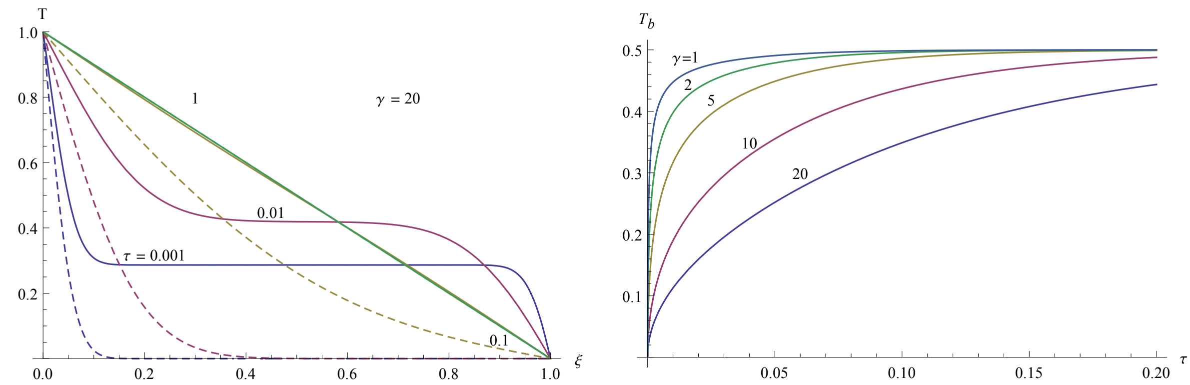

Figure 3. Temperature profile without piston effect for Dirichlet (left) and Temporal variation of bulk temperature for the Dirichlet case (right)

It can be seen by comparing the dashed lines and their corresponding full lines that the piston effect generates a great temperature increase compared to the pure thermal diffusion. Consequently, the bulk temperature of the fluid reaches steady state much more quickly when the piston effect is present. Figure 3 shows this effect where the numbering of the curves represent the variation of γ from $1, 2, 5, 10$ and 20.

Once the stronger is the Dirichlet boundary condition when it comes to heat transfer, it is expected that the same change by conditions of Neumann and Robin heating fluid becomes slower. In fact, as Robin is a mix between the conditions of Dirichlet and Neumann it is possible to predict that it provides a greater warming than Neumann, but smaller than Dirichlet. In practice, Type 1 » Type 2> Type 3. And this is exactly what happens, the types of conditions 2 and 3 (Neumann and Robin) are much closer between them graphically than type 1 of conditions (Dirichlet).

The following shows the same sequence of graphics, but this time changing the boundary condition on the right wall to Neumann (steady flow).

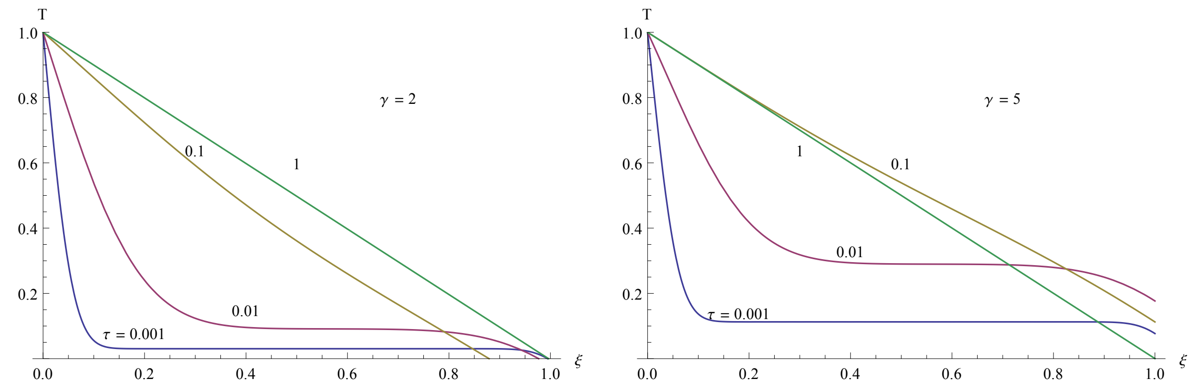

Figure 4. Local temperature profiles for a Neumann boundary condition at the right wall. $\gamma = 2$ (left) and $\gamma = 5$ (right)

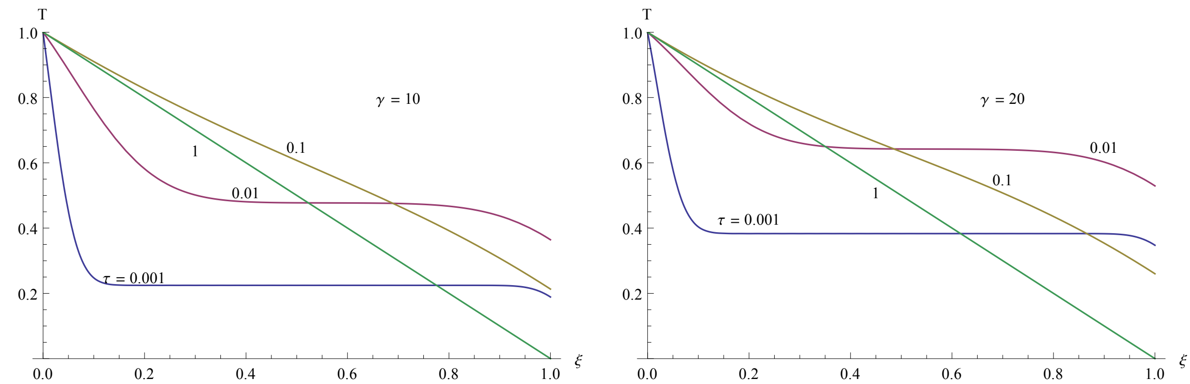

Figure 5. Local temperature profiles for a Neumann boundary condition at the right wall. $\gamma = 10$ (left) and $\gamma = 20$ (right)

As the γ increases, we can see situations where the fluid temperature rises beyond its steady state. This overheating of the fluid has a physical explanation. As the temperature is not prescribed in the right wall, the thermal boundary layer near this region is much smaller than before, and so, the transferred energy of the fluid for the boundary layer it is also much smaller. This stored energy ends up heating the entire fluid. We can note that for the biggest γ ($\gamma = 20$), the curve of the boundary layer for $t/t_{PE} = 0.001$ is very small, and the curve for $t/t_{PE} = 0.1$, it is imperceptible. Over time the fluid diminishes its temperature to reach steady state. The next graph shows what was discussed.

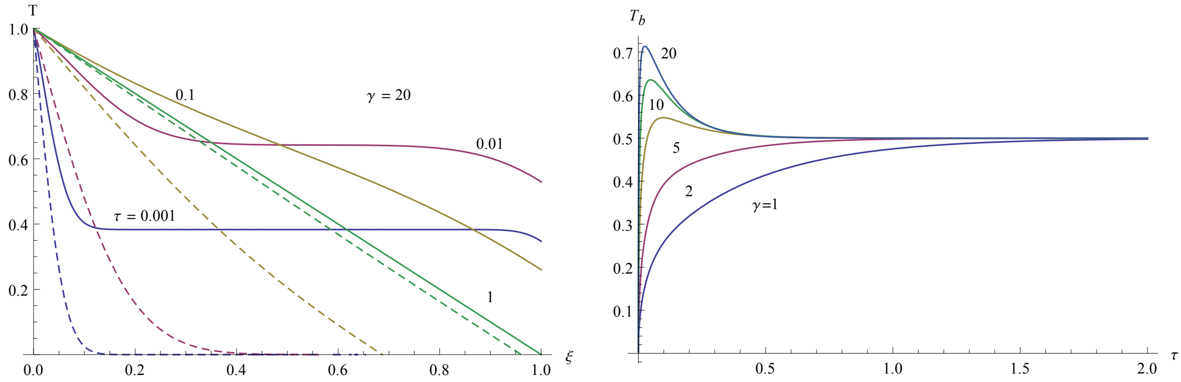

Figure 6. Temperature profile without piston effect for Neumann (left) and Temporal variation of bulk temperature for the Neumann case (right)

Now the Dirichlet-Robin case will be analyzed. The graphics of this condition have been made and are represented below. These have always been produced keeping $Bi = 1$, although it is possible to change this value. It's been done in other studies, such as Leonardo, 2012. In this work, it was observed that by increasing the Biot number, the heat transfer was stronger. It must be remembered that when $Bi = 0$, we are led to the Neumann condition, while $Bi = \infty$ leads the condition of Dirichlet.

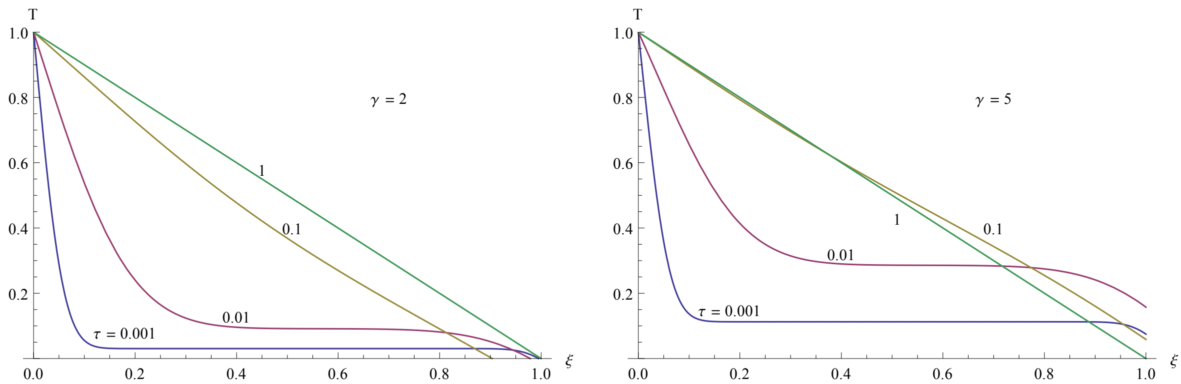

Figure 7. Local temperature profiles for a Robin boundary condition at the right wall. $\gamma = 2$ (left) and $\gamma = 5$ (right)

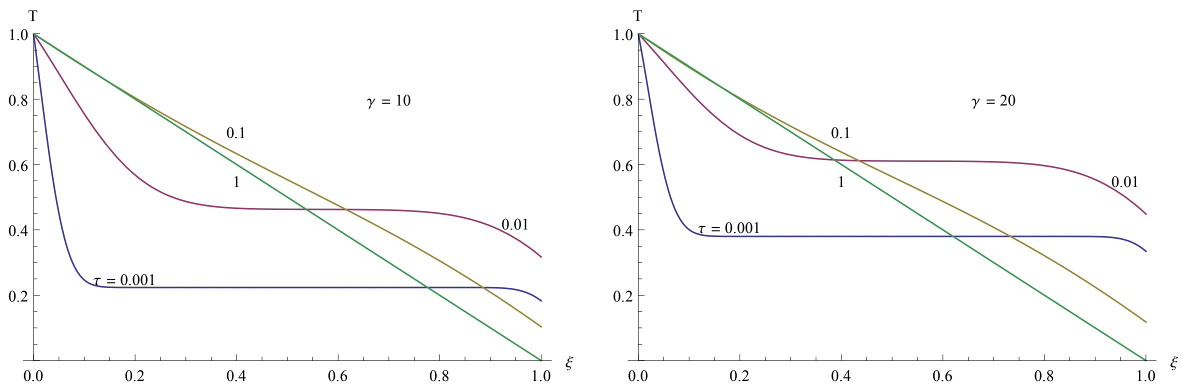

Figure 8. Local temperature profiles for a Robin boundary condition at the right wall. $\gamma = 10$ (left) and $\gamma = 20$ (right)

The same analysis for the above combination is valid for this. However, graphs do not show a greater heating than in the case Neumann, which is intriguing. The phenomenon can be explained when taking into consideration the heat transfer from the fluid to the right wall boundary layer. As with Neumann boundary layer expands more slowly, the energy that the fluid gives to this boundary layer is smaller and the way found by him dispels it is in the form of heat. With this in mind, becomes natural to imagine that when Robin is set on the right wall and the boundary layer expands more easily, bulk temperature grows more sluggish.

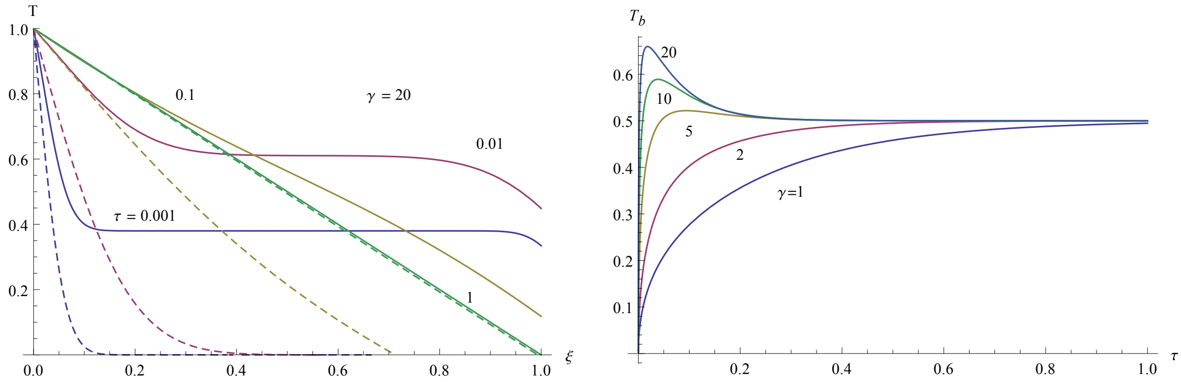

Figure 9. Temperature profile without piston effect for Robin (left) and Temporal variation of bulk temperature for the Robin case (right)

5. CONCLUSIONS

This study showed successfully the application of a thermodynamic model to analyze the behavior of the temperature of a supercritical fluid within a confined cavity 1D, varying the boundary conditions of the first, second and third type on the right wall. During the investigation results, interesting physical situations were found where the fluid temperature increased beyond the set temperature at steady state. It was possible to analyze the development of the average temperature of the system through graphics, allowing a general comparison of the possibilities.

6. REFERENCES

Barmatz, M., Hahn, I., Lipa, J.A. and Duncan, R.V., 2007. “Critical phenomena in microgravity: Past, present and future”. *Reviews of Modern Physics*, Vol. 79, pp. 1–52.

Boukari, H., Shaumeyer, J.N., Briggs, M.E. and Gammon, R.W., 1990. “Critical speeding up in pure fluids”. *Physical Review A*, Vol. 41, No. 4, pp. 2260–2263.

Carlès, P., 2010. “A brief review of the thermophysical properties of supercritical fluids”. *The Journal of Supercritical Fluids*, Vol. 53, pp. 2–11.

Carlès, P., Zhong, F., Weilert, M. and Barmatz, M., 2005. “Temperature and density relaxation close to the liquid-gas critical point: An analytical solution for cylindrical cells”. *Physical Review E*, Vol. 71, p. 041201.

Cotta, R.M., 1993. *Integral Transforms in Computational Heat and Fluid Flow*. CRC Press, Boca Raton, FL.

Ferrell, R.A. and Hao, H., 1993. “Adiabatic temperature changes in a one-component fluid near the liquid-vapor critical point”. *Physica A*, Vol. 197, pp. 23–46.

Garrabos, Y., Bonetti, M., Beysens, D., Perrot, F., Fröhlich, T., Carlès, P. and Zappoli, B., 1998. “Relaxation of a supercritical fluid after a heat pulse in the absence of gravity effects: Theory and experiments”. *Physical Review E*, Vol. 57, No. 5, pp. 5665–5681.

Huang, Y. and Bau, H.H., 1997. “Thermoacoustic waves in a confined medium”. *International Journal of Heat and Mass Transfer*, Vol. 40, No. 2, pp. 407–419.

Mikhailov, M.D. and Özisik, M.N., 1984. *Unified Analysis and Solutions of Heat and Mass Diffusion*. John Wiley & Sons, New York.

Moler, C. and Loan, C.V., 2003. “Nineteen dubious ways to compute the exponential of a matrix, twenty-five years later”. *SIAM Review*, Vol. 45, No. 1, pp. 1–46.

Nitsche, K. and Straub, J., 1987. “The critical hump of cv under microgravity, results from d-spacelab experiment”. In *Proceedings of the 6th European Symposium on Material Sciences under Microgravity Conditions*. ESA SP-256.

Onuki, A. and Ferrell, R.A., 1990. “Adiabatic heating effect near the gas-liquid critical point”. *Physica A*, Vol. 164, pp. 245–264.

Onuki, A., Hao, H. and Ferrell, R.A., 1990. “Fast adiabatic equilibration in a single-component fluid near the liquid-vapor critical point”. *Physical Review A*, Vol. 41, No. 4, pp. 2256–2259.

Özisik, M.N., 1993. *Heat Conduction*. Wiley Interscience, New York, 2nd edition.

Teixeira, P.C. and de B. Alves, L.S., 2015. “Modeling supercritical heat transfer in compressible fluids”. *International Journal of Thermal Sciences*, Vol. 88, pp. 267–278.
Zappoli, B., 2003. “Near-critical fluid hydrodynamics”. *Comptes Rendus Mecanique*, Vol. 331, pp. 713–726.

7. RESPONSIBILITY NOTICE

The authors are the only responsible for the printed material included in this paper.